J. Fluid Mech. (2009), *vol.* 628, *pp.* 155–180.
doi:10.1017/S0022112009006144 Printed in the United Kingdom

Acoustic resonances and trapped modes in annular plate cascades

WERNER KOCH†

Institute of Aerodynamics and Flow Technology, DLR Göttingen 37073, Germany

(Received 20 August 2008 and in revised form 16 January 2009)

As a stepping stone towards understanding acoustic resonances in axial flow compressors, acoustic resonances are computed numerically in fixed single and tandem plate cascades in an infinitely long annular duct. Applying perfectly matched layer absorbing boundary conditions in the form of the complex scaling method of atomic and molecular physics to approximate the radiation condition the resonance problem is transformed into an eigenvalue problem. Of particular interest are resonances with zero radiation damping (trapped modes) or very small radiation damping (nearly trapped modes). Such resonances can be excited by wakes from compressor cascades or struts. If the shedding frequency is sufficiently close to an acoustic resonant frequency, the latter may control the vortex shedding causing high-intensity tonal noise or occasionally even blade failure. All resonances are computed for zero mean flow approximating low-Mach-number flows. The influence of various cascade parameters on the resonant frequencies is studied and, whenever possible, our numerical results are compared with published experimental findings.

1. Introduction

Based on observations of blade vibrations, which could neither be attributed to blade resonances nor blade flutter in several commercial compressors, Parker and his colleagues conducted a series of experiments with straight (Parker 1966; Parker & Griffiths 1968) and annular cascades (Parker 1967*a*; Parker & Pryce 1974). These experiments demonstrated conclusively that vortices shed periodically in the wake of thin plates or blades in a cascade can be enhanced considerably by acoustic resonances leading to high-intensity discrete frequency noise and/or blade vibrations. Parker pointed out that contrary to the opinion held up to that time, these resonances are controlled by the geometry of the system and not the natural frequencies of mechanical blade vibrations (their main findings are nicely reviewed in Parker & Stoneman 1989). Similar resonant acoustic phenomena were observed in single-stage axial flow compressors by Parker (1968) in multistage axial flow compressors by Camp (1999) and Hellmich (2008) (see also Hellmich & Seume 2008) as well as in centrifugal compressors by Ziada, Oengören & Vogel (2002).

An essential result of Parker's experiments was that these resonant acoustic modes appeared to decay exponentially upstream and downstream from the cascade. Using this exponential decay property Parker (1967*b*) was able to compute the resonant frequencies and modes for a single infinitely thin plate in a wind tunnel by a relaxation method. These standing wave modes are now commonly referred to as Parker modes

† Email address for correspondence: werner.koch@dlr.de

and were fully confirmed by further experiments of Cumpsty & Whitehead (1971). It should be emphasized that in the experiments even fully turbulent wakes were coordinated into coherent vortex-street-like eddies by these acoustic resonances.

In the context of water waves, Evans & Linton (1991) (see also Evans 1992) rediscovered these Parker modes and Evans *et al.* (1994) gave a rigorous mathematical proof for the existence of the Parker modes showing that they have zero radiation loss and are trapped near the finite-length plate in the duct. Therefore, the Parker modes are an example of so-called *trapped modes* defined as strongly localized resonant modes with zero radiation loss. In the theory of water waves, Ursell (1951) was the first to establish the existence of trapped modes. In quantum waveguides trapped modes are known as bound states, cf. Duclos & Exner (1995) or Linton & Ratcliffe (2004). Similar trapped modes are found in electromagnetic waves, cf. Porter & Evans (1999), and elastic waves, see, for example, Porter (2007). Mathematically the existence of truly trapped modes is of considerable interest because it means that there exists an eigenfunction of the homogeneous problem which makes the solution of the forced scattering or radiation problem non-unique. In practical engineering trapped modes with zero damping, or nearly trapped modes (in electromagnetic multilayer structures these modes are termed 'defect modes') with very small damping, are of great importance because a small radiation damping can lead to a high-amplitude response if excited by time-periodic sources causing annoying noise and/or structural damage. Trapped modes became the subject of renewed interest after numerical computations of Maniar & Newman (1997) showed unusually high loads at particular frequencies of water waves impinging on a row of equally spaced circular cylinders, and much effort has gone into providing both rigorous existence proofs as well as numerical evidence for the presence of trapped or nearly trapped modes.

Starting with the original paper of Parker (1967*b*) various early publications were devoted to the actual computation of resonances and trapped modes. Guided by his experimental data Parker (see also Parker & Stoneman 1985) solved the Helmholtz equation numerically by fixing the location of the nodes and applying a Dirichlet boundary condition a finite distance away from the plate. Unless one has actual proof that the modes are truly trapped, this can lead to erroneous results: for example, Koch (1983) showed that the trapped Parker modes become damped resonances if the mean flow Mach number is finite (compare also Duan 2004). For the computation of these damped resonances a radiation condition, allowing only outgoing waves, has to be employed whereas application of a Dirichlet boundary condition a finite distance away from the plate gives unphysical reflections, which falsify the results. Therefore, the prevailing approach has been to solve the time-periodic scattering problem and search for solutions of the homogeneous problem as the amplitude of the incoming wave approaches zero. Usually this leads to an infinite system of equations which can be truncated and the determinant of which has to vanish. Examples are the mode-matching results of Nayfeh & Huddleston (1979), Evans & Linton (1994) and Duan (2004); the Wiener–Hopf results of Koch (1983), Evans & Linton (1991) and Woodley & Peake (1999*a*) or the multipole expansions of Ursell (1951) and Callan, Linton & Evans (1991). If one can show that there exist resonances with zero damping, this can be used as constructive existence proof of trapped modes. The disadvantage of all above mentioned (semi-analytic) solution methods is that they are only applicable for very special geometries.

Recently, Hein, Hohage & Koch (2004) proposed a method for the numerical computation of resonances by approximating the radiation condition via perfectly

matched layer (PML) absorbing boundary conditions. Using, for example, a finite element approximation the resonances of an arbitrary object in an unbounded domain can thereby be found by solving a (large) linear generalized eigenvalue problem (the frequency-dependent PML formulation of Bérenger (1994) requires the solution of a nonlinear eigenvalue problem). In a series of papers Koch (2005), Hein *et al.* (2007), Duan *et al.* (2007) and Hein & Koch (2008) applied this method successfully to various two- and three-dimensional open domain problems. Trapped modes with zero radiation loss are only possible for objects in laterally bounded domains. However, it should be stressed that the numerical method of Hein *et al.* (2004) cannot give a mathematically rigorous proof for the existence of truly trapped modes. But if the damping of the resonance can be reduced to very low values by refining the numerical grid, this is usually a strong indication for the existence of a trapped or nearly trapped mode. From a practical point of view it does not matter whether the mode is truly trapped or merely nearly trapped as long as the damping is very small, which is equivalent to a high-quality-factor resonance.

The primary objective of the present paper is to predict the acoustic resonances (resonant frequencies and radiation damping) of plate cascades in an annular duct modelling the situation in axial flow compressors. Of particular interest are trapped or nearly trapped modes with vanishingly small radiation damping. Instead of selecting a specific compressor blade geometry we consider in the first part a single annular plate cascade which was investigated experimentally by Parker & Pryce (1974), and examine the influence of various cascade parameters on the trapped mode frequencies. As trapped modes exist only for frequencies below the corresponding duct cutoff frequency, they cannot be excited linearly via incoming duct waves (recently Li & Mei (2006) showed that trapped modes can be excited subharmonically by an incident wave of twice the eigenfrequency). Parker identified periodic vortices shed in the wake of blunt-edged blades as the main source exciting trapped modes in his experiments. Such vortices are shed normally at comparatively high frequencies. However, Parker (1984) also indicated that vortices shed from fully or partially stalled blade rows could be another source of excitation at off-design conditions and at much lower frequencies.

Parker (1997) indicated that acoustic resonances have caused blade failures in high-speed multistage compressors during aero-engine research and development in the early eighties, but for proprietary reasons almost no data have been published in the open literature. Legerton (1992) analysed relevant acoustic resonance phenomena in several full-scale Rolls Royce research compressors but it can be assumed that similar problems have been encountered by other aero-engine manufacturers. Recently, acoustic spinning mode resonances were observed by Ulbricht (2002) in her experimental investigation of compressor stability in stationary annular cascades, and Hellmich (2008) found spinning mode resonances close to the stall limit of a four-stage axial flow compressor. To state it clearly, the forcing mechanism as well as the highly nonlinear process of frequency locking at resonance is not subject of this investigation. Here we merely compute the acoustic trapped or nearly trapped mode frequencies which might enhance any existing periodic source of comparable frequency and demonstrate how the resonant frequencies depend on various cascade parameters. All above mentioned source mechanisms require a mean flow. However, Koch (1983) showed that for low Mach numbers the influence of mean flow on the acoustic resonances is negligibly small, and we therefore compute the resonances for zero mean flow.

In the second part of our paper we compute the resonances in stationary tandem cascades. Stoneman *et al.* (1988) examined the acoustic resonances of tandem plates in a rigid-walled rectangular duct experimentally and computationally. Legerton (1992) performed additional tests with tandem plates. They found strong enhancement of the discrete-frequency noise if the vortex shedding frequency was close to the resonant acoustic frequency analogous to the single-cascade Parker modes. Similar effects are expected in a compressor stage. Modelling an idealized compressor stage, Legerton (with first results published in Legerton, Stoneman & Parker 1991) investigated stationary annular tandem cascades experimentally and found that the plate spacing affected both the amplitude of the sound produced as well as the frequency at which the resonance was excited. Extending the single-plate Wiener–Hopf analysis of Koch (1983) to two-dimensional tandem cascades Woodley & Peake (1999*a*) computed the resonant frequencies for one of the geometries investigated by Legerton and found good agreement despite neglecting blade thickness and curvature of the duct passage. In the present paper we include blade thickness and consider the annular geometry but neglect the mean flow.

The paper is organized as follows: after a brief outline of the solution method in § 2 we reconsider resonances of radial fins in a circular duct in § 3. In § 4 we examine single annular plate cascades and study the influence of various cascade parameters on the resonant frequencies. Tandem plates and stationary tandem cascades are treated in § 5 and a summary concludes the paper.

2. Governing equation and solution procedure

The equation governing acoustic disturbances in a medium with zero mean flow is the wave equation. In the following all lengths will be non-dimensionalized with a characteristic reference length l^*_{ref}, velocities with the ambient speed of sound c^*_0, densities with the ambient density ρ^*_0 and pressures with $\rho^*_0 c^{*2}_0$. Here the asterisk superscript denotes a dimensional quantity. Assuming periodic time dependence $\exp(-\mathrm{i}\omega^* t^*)$, where ω^* is the circular frequency, the wave equation can be reduced to the Helmholtz equation:

$$\Delta\phi(x, y, z) + K^2\phi(x, y, z) = 0, \tag{2.1}$$

for the (non-dimensional) velocity potential $\phi(x, y, z)$. $\Delta = \partial^2/\partial x^2 + \partial^2/\partial y^2 + \partial^2/\partial z^2$ is the three-dimensional Laplacian in (non-dimensional) Cartesian coordinates x, y, z; and $K = \omega^* l^*_{ref}/c^*_0$ denotes the dimensionless frequency, with $K/2\pi$ being the Helmholtz number. The time-independent dimensionless disturbance velocity and pressure are then given by $v(x, y, z) = \nabla\phi$ and $p(x, y, z) = \mathrm{i}K\phi$, respectively. On the duct walls as well as on all plates we impose the Neumann boundary condition

$$\frac{\partial\phi}{\partial n} = 0, \tag{2.2}$$

for sound-hard walls. The formulation of the problem is completed by imposing a radiation condition allowing only outgoing waves.

In a numerical treatment the implementation of the radiation condition constitutes a main difficulty because numerical computations are necessarily conducted on truncated domains. At these finite grid boundaries unphysical reflections occur, often causing large errors in the solution, unless special boundary conditions are applied on the surface bounding the computational domain. Basically, there are two methods to overcome this problem: the first uses so-called non-reflecting boundary

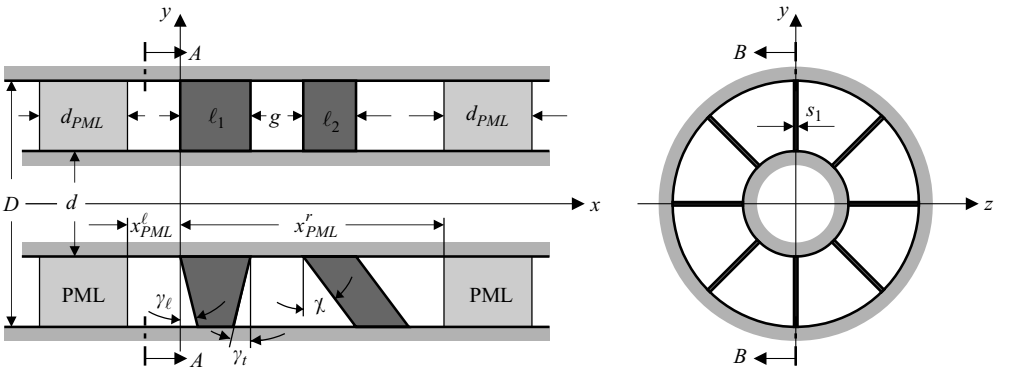

FIGURE 1. Sketch of tandem cascade of plates (upper half of left figure) or single cascade of tapered or swept plates (lower half of left figure) in annular duct with PMLs.

conditions on the surface bounding the computational domain. Analysing the problem outside the truncated computational domain a relation can be established involving the unknown solution and its derivative. This so-called Dirichlet-to-Neumann (DtN) map is then used as boundary condition for the interior computational domain (see, for example, Harari, Patlashenko & Givoli 1998).

The second method employs absorbing boundary conditions by adding a non-physical layer which absorbs outgoing waves without reflection. PML absorbing boundary conditions were introduced by Bérenger (1994) and became increasingly popular in electromagnetic and acoustic problems (for a recent review in acoustics see Hu 2004). Instead of the frequency-dependent PML formulation of Bérenger, cf. the complex coordinate stretching formulation of Chew & Weedon (1994), Hein *et al.* (2004) used the much older complex scaling method of atomic and molecular physics with frequency-independent PML coefficients. The complex scaling method, introduced by Aguilar & Combes (1971), Baslev & Combes (1971) and Simon (1973), cf. the monograph by Hislop & Sigal (1996) or the recent review by Moiseyev (1998), makes use of the fact that the PML eigenvalues for the infinite domain problem coincide with the resonances of the original problem for rather general PML scalings. In a recent paper Kim & Pasciak (2009) proved that the eigenvalues of the truncated PML problem (a necessity for the numerical approach) converge to the desired resonances as the PML domain increases.

In the present paper we shall apply the complex scaling method to the computation of acoustic resonances in single or tandem plate cascades in an annular duct as depicted in figure 1. An annular duct with outer diameter D and inner diameter d contains a single or tandem cascade of finite thickness plates. The N_1 evenly distributed plates of the first cascade are of length l_1 and thickness s_1, the N_2 plates of the second cascade are of length l_2 and thickness s_2 with a gap g between the two cascades. The plates can be tapered with a leading-edge taper angle γ_l and a trailing-edge taper angle γ_t or swept with a sweep angle χ as sketched in figure 1. Furthermore, the plates can be staggered with a stagger angle α where $\alpha = 0$ for an unstaggered cascade.

In the following we provide a brief overview of how the PML works: in the annular PML domain in front and behind the tandem cascade, see figure 1, $\phi(x, y, z)$ is continued analytically with respect to the axial variable x to the complex variable ξ, e.g.

$$\xi(x) = x + \mathrm{i}\sigma(x). \tag{2.3}$$

The spatial damping function $\sigma(x)$ is usually chosen in power form, smoothly starting at the PML interfaces at $x = x^r_{PML}$ and $x = -x^l_{PML}$ respectively:

$$\sigma(x) = \begin{cases} \sigma_0 (x - x^r_{PML})^\beta, & x > x^r_{PML}, \\ 0, & -x^l_{PML} \leqslant x \leqslant x^r_{PML}, \\ -\sigma_0 (-x - x^l_{PML})^\beta, & x < -x^l_{PML}. \end{cases} \tag{2.4}$$

For a positive damping coefficient σ_0 and a constant shape parameter $\beta \geqslant 1$ (we chose $\beta = 1$ for all our computations, cf. Hein *et al.* 2004) outgoing waves will decay exponentially in the PML. One can therefore truncate the PML at $(x^r_{PML} + d_{PML})$ and $-(x^l_{PML} + d_{PML})$, where d_{PML} denotes the width of the PML. The error due to artificial reflections at this truncated outer edge of the PML is small if σ_0 and d_{PML} are chosen properly (in general we chose $\sigma_0 = 2$ and $d_{PML} \geqslant 2$). Therefore, a Dirichlet boundary condition can be imposed at the outer edge of the PML instead of enforcing the radiation condition, cf. Collino & Monk (1998). In this way a finite domain eigenvalue problem results which can be solved numerically by standard methods. In this paper we apply the high-order finite-element code NGSolve of Joachim Schöberl together with his grid generation code NETGEN, cf. Schöberl (1997), and solve the ensuing large eigenvalue problem with a shifted Arnoldi algorithm. The accuracy of the finite-element solution is controlled by the maximal mesh size Δ of the grid and the order p of the finite element polynomial on an individual triangle. For three-dimensional objects the number of degrees of freedom N_{dof} in the finite-element formulation, and correspondingly the storage requirements, are quite large such that we use $p = 2$ in almost all our calculations. Only for occasional accuracy checks we increase p to $p = 3$. In NGSolve the mesh size Δ can be varied locally. For example, we chose a much coarser mesh in the PML denoted by the second number for Δ.

3. Radial fins in cylindrical duct

To demonstrate the applicability of our numerical method for the prediction of standing as well as spinning mode resonances, we first compute the resonances in a cylindrical duct with N uniformly distributed radial fins of finite chord l/D and with finite thickness s/D. In circular and annular ducts the appropriate reference length $l^*_{ref} = D^*$. For this problem Linton & McIver (1998) predicted trapped standing waves using the mode-matching method and in a follow-up paper Duan & McIver (2004) proved the existence of additional trapped spinning modes by means of Bloch theory. The term spinning mode for a steady pressure pattern which rotates was first introduced by Tyler & Sofrin (1962), and a finite number of trapped spinning modes was observed experimentally by Parker & Pryce (1974) in a stationary annular cascade. Duan & McIver showed that if the number of fins N is even, then $N/2 + 1$ families of trapped modes exist with a fixed number of nodal lines n in axial direction, while for N odd $(N - 1)/2 + 1$ families of trapped modes are possible. This is analogous to the existence of trapped modes in a two-dimensional channel containing N uniformly distributed structures as investigated by Utsunomiya & Eatock Taylor (1999), Linton & McIver (2002) and Porter & Evans (1999).

First we choose $N = 4$ but instead of using infinitely thin fins, as used by Linton & McIver (1998) and Duan & McIver (2004), we allow fins of finite thickness s assuming arbitrarily $s/D = 0.04$. Resonant modes may be classified by three numbers (m, n, ρ): the circumferential mode number m, being the number of wavelengths around the circumference, and n and ρ denoting the number of nodal lines in axial and radial

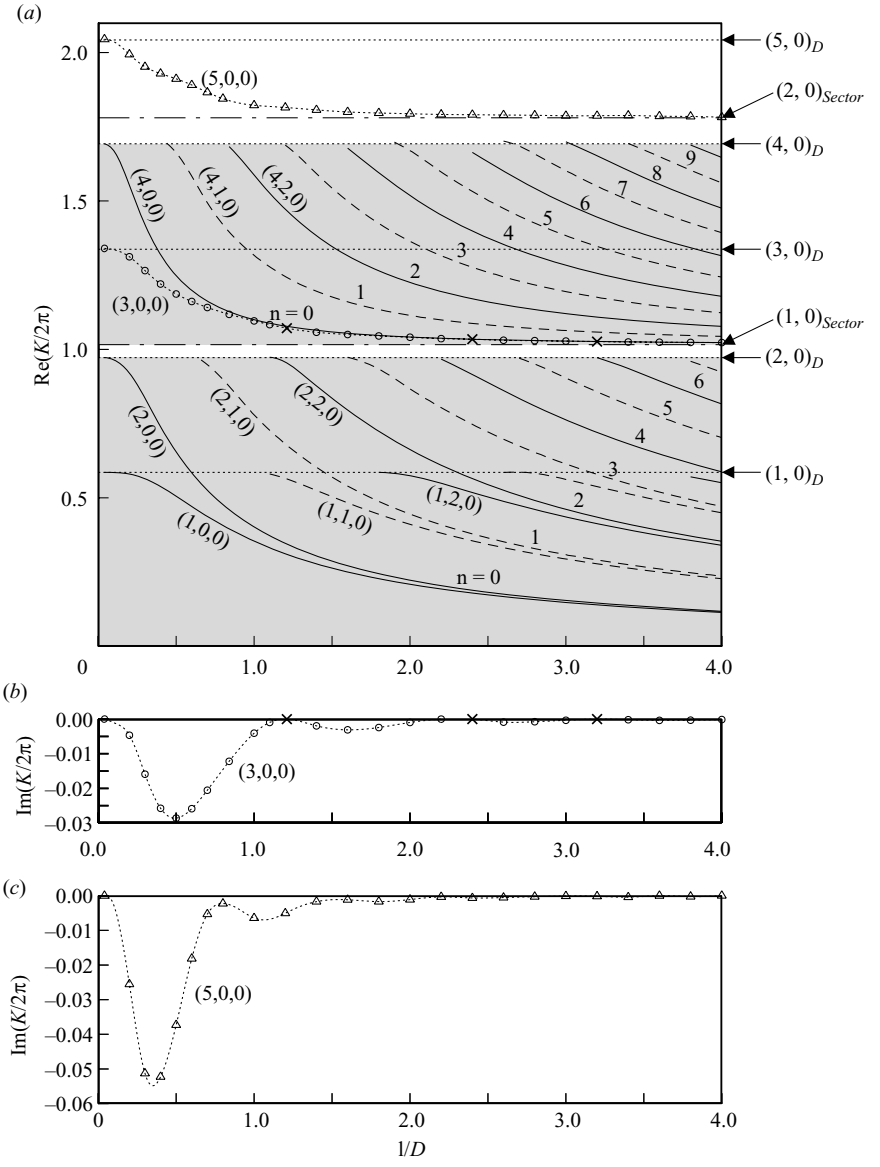

FIGURE 2. Circular cylindrical pipe with $N=4$ radial fins of thickness $s/D=0.04$: (*a*) resonant frequencies $\mathrm{Re}(K/2\pi)$ and (*b*) damping $\mathrm{Im}(K/2\pi)$ of $(3,0,0)$ and (*c*) of $(5,0,0)$ mode as function of fin chord length l/D. Full lines mark x-symmetric trapped modes, dashed lines mark x-antisymmetric trapped modes. $p=2$, $d_{PML}=4$, $\sigma_0=2$, $\Delta=0.06/0.16$.

directions, respectively. By assuming either symmetry ($n=0, 2, \ldots$) or antisymmetry ($n=1, 3, \ldots$) about $x=0$ we may limit our computation to the half problem $x \geqslant 0$. The results of our computation are shown in figure 2.

As postulated by Duan & McIver (2004), three families of trapped modes exist for $N=4$ radial fins which they denoted by $p=0, 1, 2$. Their first two families $p=1$ and $p=2$ start at the $(1,0)_D \approx 0.5861$ and $(2,0)_D \approx 0.9722$ cutoff frequencies $(m,\rho)_D$ of the circular pipe and end at $\mathrm{Re}(K/2\pi)=0$ for $l/D \to \infty$. The cutoff frequencies $(m,\rho)_D$ are simply $j'_{m,\rho}/\pi$, where $j'_{m,\rho}$ is the ρth zero of $J'_m(x)$. Here $J_m(x)$ is the Bessel

function of the first kind. Values of $j'_{m,\rho}$ are listed, for example, in Abramowitz & Stegun (1965, p. 411). In our figure 2(a) all cutoff frequencies $(m,0)_D$ of the circular pipe modes are marked by the dotted lines and are denoted on the right-hand side of figure 2(a). The $p=0$ family of Duan & McIver starts at the cutoff frequency $(4,0)_D \approx 1.6926$ and ends at the cutoff frequency denoted by $(1,0)_{Sector} \approx 1.016$ on the right-hand side of figure 2(a). $(1,0)_{Sector}$ is the cutoff frequency of the mode with one nodal line in circumferential direction in the sector between two infinitely long fins and zero nodal lines in radial direction. In our figure 2 the cutoff frequencies $(m,0)_{Sector}$ are marked by the dash-dotted lines that are computed numerically as the beginning of the continuous spectra using PMLs for fins, which are infinitely long in axial direction. The shaded areas mark the domains of trapped modes. We notice that by using fins of finite thickness there is a small gap between the two shaded areas which does not exist for the infinitely thin fin results of Duan & McIver because for infinitely thin fins $(2,0)_D$ coincides with $(1,0)_{Sector}$.

Resonant modes $(3,n,0)$ also exist. They start at $(3,0)_D \approx 1.3373$ and end at $(1,0)_{Sector}$ (only the $(3,0,0)$ mode is shown in figure 2 by the dotted curve with the circular symbols). As can be seen from the damping in figure 2(b) the $(3,0,0)$ mode is not trapped. (The damping is controlled by the imaginary part $\mathrm{Im}(K/2\pi)$ of the frequency and is closely related to the quality factor $Q=|\mathrm{Re}(K)/(2\mathrm{Im}(K))|$ of the resonator defined as the ratio of stored energy to dissipated energy.) But it looks like there exist embedded trapped modes at the particular l/D values marked by the cross symbols in figure 2. With our numerical method we cannot prove the existence of an embedded trapped mode, but by the method of bisection we could reduce the damping of the $(3,0,0)$ mode to very low values at these particular l/D values which is a strong indication that these might indeed be truly embedded trapped modes. To a certain degree this would be analogous to the embedded trapped modes found by Duan *et al.* (2007) for the two-dimensional infinite cascade problem. The $(5,0,0)$ mode, depicted by the dotted curve with triangular symbols in figure 2, only shows nearly trapped modes at the points with minimal damping and ends at $(2,0)_{Sector} \approx 1.780$ for $l/D \to \infty$. In our numerical computation spinning modes can be recognized as double eigenvalues with corresponding eigenfunctions which are phase shifted by 90°. For example, the $(1,n,0)$ modes are double eigenvalues while the $(2,n,0)$ and $(4,n,0)$ modes are simple eigenvalues and therefore standing waves.

Next, we consider the 8-fin case. For $N=8$ and infinitely thin plates, Linton & McIver (1998) computed the standing wave solutions and found a fundamental change from the $N=4$ case, namely the occurrence of so-called avoided crossings or near intersections of two families of eigenvalues. Berry & Wilkinson (1984) explained this phenomenon as degeneracy of real eigenvalues near a so-called diabolical point where the eigenvalue surface forms a double cone. Varying the eigenvalues as function of one parameter (in our case l/D) near a diabolical point, the avoided crossings are approximately double-hyperbola curves obtained by slicing the double cone near its vertex. For the eigenvalue curves to pass exactly through a diabolical point, a second parameter is required. Another reason for looking at the 8-fin case is that Parker & Pryce (1974) used eight plates in their annular cascade experiment with a plate thickness of $s/D=0.02$. For this reason we also choose $s/D=0.02$, contrary to the infinitely thin plates of Linton & McIver. Prescribing symmetry or antisymmetry about $x=0$ we may again limit our computation to the half problem $x \geqslant 0$. The results of this computation are depicted in figure 3 for $0 \leqslant l/D \leqslant 2$.

According to Duan & McIver (2004) five families of trapped modes exist for $N=8$ including the spinning modes. All trapped modes start at the pipe cutoff frequencies

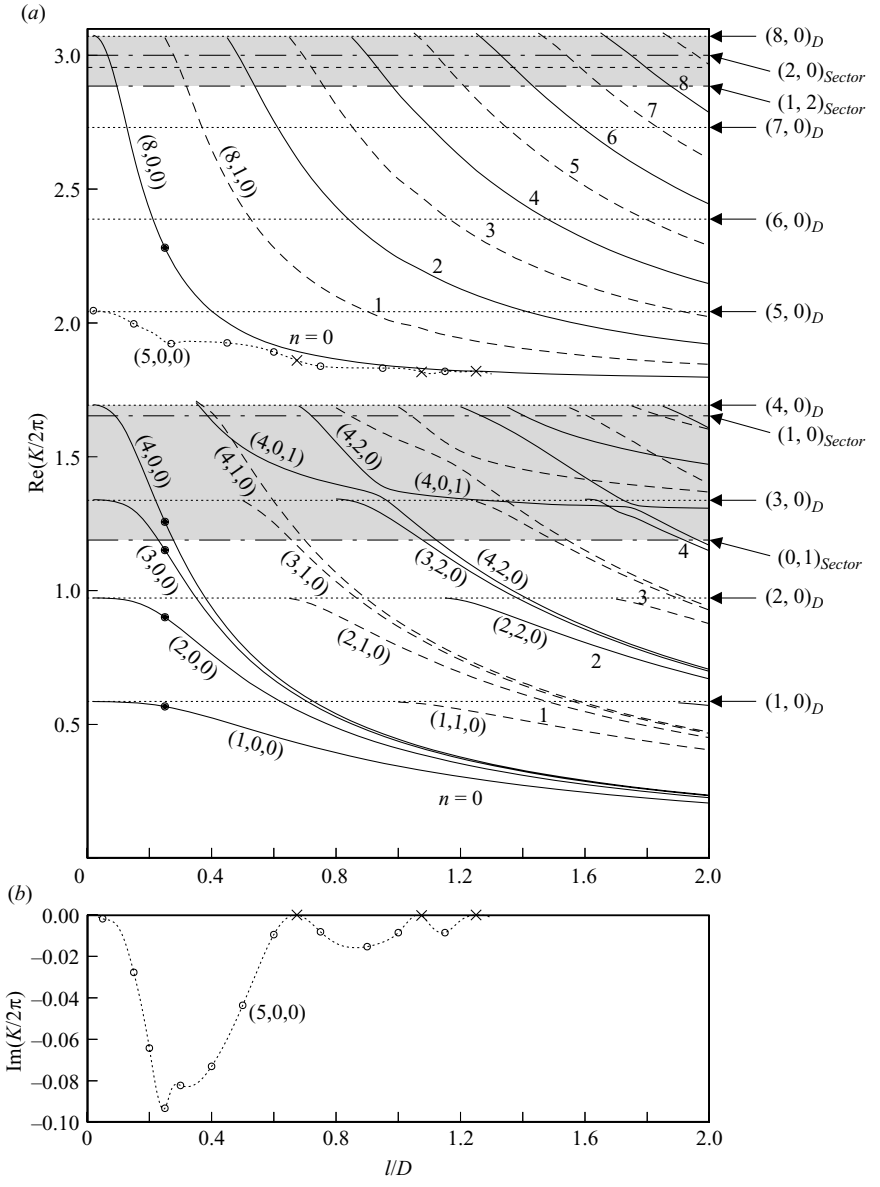

FIGURE 3. Circular cylindrical pipe with $N = 8$ radial fins of thickness $s/D = 0.02$: (*a*) resonant frequencies $\mathrm{Re}(K/2\pi)$ and (*b*) damping $\mathrm{Im}(K/2\pi)$ of $(5, 0, 0)$ mode as function of fin chord length l/D. Full lines mark x-symmetric trapped modes, dashed lines mark x-antisymmetric trapped modes. $p = 2$, $d_{PML} = 2$, $\sigma_0 = 2$, $\Delta = 0.06/0.16$.

$(m, 0)_D$ marked on the right-hand side of figure 3(*a*). The first four families start at $(1, 0)_D, \ldots, (4, 0)_D$ and end at $\mathrm{Re}(K/2\pi) = 0$ for $l/D \to \infty$ whereas the fifth family starts at $(8, 0)_D \approx 3.0709$ and approaches $\mathrm{Re}(K/2\pi) = (1, 0)_{Sector} \approx 1.653$. The modes starting at $(5, 0)_D$, $(6, 0)_D$ and $(7, 0)_D$ are damped resonances as can be seen for the depicted $(5, 0, 0)$ mode. With the resolution limited by the storage of our desktop computer it is difficult to distinguish the various eigenfunctions for higher l/D and

$\mathrm{Re}(K/2\pi)$, but it appears that at particular values of l/D nearly trapped or perhaps embedded trapped modes occur which are marked by the cross symbols in figure 3.

Between modes with the same circumferential mode number m but different number of axial or radial nodal lines avoided crossings occur, for example, between the $(4, 2, 0)$ mode and the $(4, 0, 1)$ mode. This is possible because between $(4, 0)_D$ and $(0, 1)_{Sector} \approx 1.189$, marked by the lower shaded area in figure 3(a), not only the $(4, n, 0)$ modes are cut on but also the $(4, n, 1)$ modes. All $(m, n, 1)$ modes approach $(0, 1)_{Sector}$ as $l/D \to \infty$. It is interesting that at these avoided crossings the eigenfunctions interchange their identity, i.e. for example, the $(4, 2, 0)$ mode becomes the $(4, 0, 1)$ mode and the $(4, 0, 1)$ mode changes into a $(4, 2, 0)$ mode. Contrary to the results for infinitely thin plates, cf. figure 8 in Linton & McIver (1998), no avoided crossings are observed between $(8, 0)_D$ and $(1, 2)_{Sector}$, cf. the upper shaded area in figure 3(a). To check if our numerical discretization was inadequate, we performed a few test computations with $p = 3$ on a larger computer which confirmed our $p = 2$ results. Furthermore, the $N = 7$ results in figure 5 of Duan & McIver (2004) for infinitely thin plates show a qualitatively similar behaviour so that indeed there seem to be no avoided crossings in the shaded area between $(8, 0)_D$ and $(1, 2)_{Sector}$ for $s/D = 0.02$. Avoided crossings of eigenvalues are of considerable theoretical interest. However, they occur at larger l/D whereas for typical applications in compressor cascades l/D is much lower such that avoided crossings are of no importance there. For instance, in the annular experiment of Parker & Pryce (1974) $l/D = 0.25$, and we marked the trapped mode frequencies for the 8-fin case at $l/D = 0.25$ by filled circles in figure 3(a) for later reference.

4. Single-plate cascade in annular duct

A real compressor has a finite hub-to-tip ratio d/D and small chord lengths l/D. Linton & McIver (1998) outlined in their § 5 how to extend their mode-matching analysis to annular cascades with infinitely thin plates and gave an approximate solution for large N. In the following we compute the resonances numerically for finite thickness plate cascades in an annular duct as depicted in figure 1. Symmetry arguments about $x = 0$ can be used to limit our computation to the half space $x \geqslant 0$. Guided by the experiment of Parker & Pryce (1974) we consider first a single annular cascade with $N = 8$ evenly distributed plates with $l/D = 0.25$ and of thickness $s/D = 0.02$ and vary the hub-to-tip ratio d/D. Starting with the $d/D = 0$ trapped mode resonances of the previous section, marked by solid circles in figure 3(a), the results of our computation are shown in figure 4. We note without proving it that the number of trapped modes remains the same as for the radial fin case with $d/D = 0$ and the trapped mode frequencies drop slightly with increasing hub-to-tip ratio d/D. For the higher order circumferential modes, the trapped mode frequencies $(m, 0, 0)$ are considerably lower than the corresponding annular duct cutoff frequencies $(m, 0)_D$ which are shown by the dotted curves in figure 4. The cutoff frequencies $(m, 0)_D$ depend on the hub-to-tip ratio $\sigma = d/D$ and are $k'^{(\sigma)}_{m,\rho}/\pi$ where $k'^{(\sigma)}_{m,\rho}$ is the ρth zero of $J'_m(x)N'_m(xd/D) - J'_m(xd/D)N'_m(x)$, cf. Appendix B in Tyler & Sofrin (1962). Here $N_m(x)$ denotes the Bessel function of the second kind. For $d/D = 1$, the resonant trapped mode frequencies approach the resonant frequencies of a corresponding two-dimensional plate cascade with periodic boundary conditions imposed at $y = 0$ and the duct perimeter $y = D\pi$ as sketched, for example, in figure 1 of Ragab & Salem-Said (2007) and the cutoff frequencies $(m, 0)_D$ approach m/π marked by the arrows

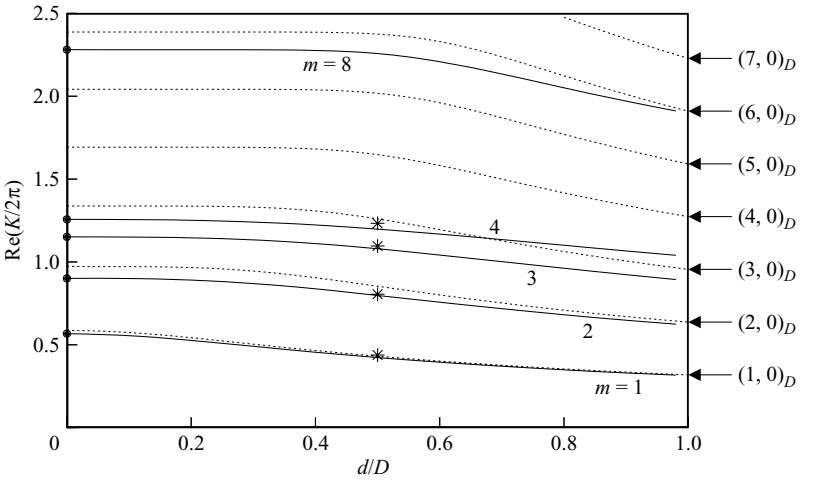

FIGURE 4. Annular cascade with $N = 8$ radial plates of chord length $l/D = 0.25$ and thickness $s/D = 0.02$: variation of frequency $\mathrm{Re}(K/2\pi)$ of trapped modes $(m, 0, 0)$ (solid curves) as well as corresponding duct cutoff frequencies (dotted curves) as function of hub-to-tip ratio d/D. The filled circular symbols show the results for the radial fins of the previous section, the asterisk symbols depict the experimental results of Parker & Pryce (1974) for $d/D = 0.5$. $p = 2$, $d_{PML} = 2$, $\sigma_0 = 2$, $\Delta = 0.06/0.16$.

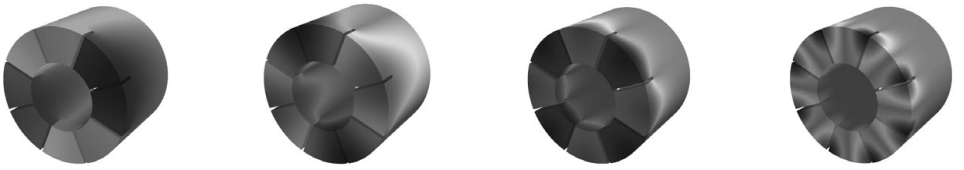

FIGURE 5. Examples of x-symmetric trapped mode eigenfunctions for the geometry of Parker & Pryce (1974): $N = 8$, $d/D = 0.5$, $l/D = 0.25$, $s/D = 0.02$. Shown are the eigenfunctions in the half plane $x \geqslant 0$ up to the downstream PML.

on the right-hand side of figure 4. Assuming $c_0^* = 340$ m s^{-1}, the asterisk symbols at $d/D = 0.5$ in figure 4 depict the experimental results of Parker & Pryce which agree fairly well with our numerical results despite the neglect of mean flow in our computation.

Whereas in the experiment of Parker & Pryce (1974) the frequency of the first circumferential trapped mode $m = 1$ could only be excited by a loudspeaker mounted at an opening in the side of the duct, the second, third and fourth trapped modes were excited by vortices shed from the trailing edges of the plates. The fifth trapped mode $m = 8$ was apparently outside the domain of their measurement. In our computation the first three trapped modes $(m, 0, 0)$, $m = 1, 2, 3$ are spinning modes whereas (4, 0, 0) and (8, 0, 0) are standing wave modes. The (4, 0, 0) mode corresponds to the 'one node per blade' mode observed in the experiments of Parker, see Parker (1968), Parker & Pryce (1974) and Parker & Stoneman (1985, 1987). Figure 5 shows examples of trapped mode eigenfunctions for the geometry of Parker & Pryce. In the following we use the experimental configuration of Parker & Pryce with $d/D = 0.5$, $l/D = 0.25$, $N = 8$,

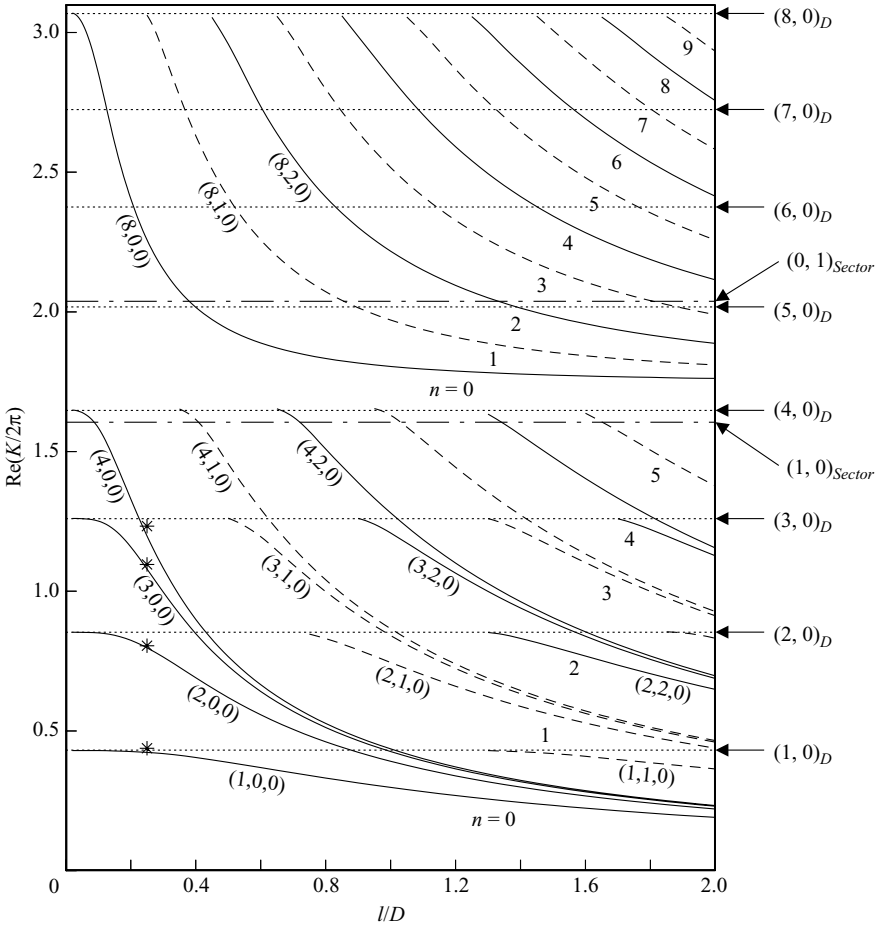

FIGURE 6. Annular cascade with $N = 8$ radial plates of thickness $s/D = 0.02$ and hub-to-tip ratio $d/D = 0.5$: variation of resonant frequencies $\mathrm{Re}(K/2\pi)$ as function of blade chord length l/D. The asterisk symbols depict the experimental results of Parker & Pryce (1974) for $l/D = 0.25$. $p = 2$, $d_{PML} = 2$, $\sigma_0 = 2$, $\Delta = 0.06/0.16$.

$s/D = 0.02$ and zero stagger angle as our reference geometry and vary individual parameters such as blade chord length, blade pitch, stagger angle or blade sweep in order to study their influence on the trapped mode resonances.

4.1. *Influence of blade chord length*

Figure 6 depicts the trapped mode resonances for $0 \leqslant l/D \leqslant 2$. In an actual compressor only the $(m, 0, 0)$ trapped modes for low l/D are of interest. We note that at these low l/D values the length of the blade chord has a strong influence on the trapped mode frequencies: with increasing l/D, in particular for larger circumferential mode numbers m, the trapped mode frequencies decrease considerably below the cutoff frequency of the corresponding annular duct mode $(m, 0)_D$. We also observe that contrary to the radial fin case of § 3 no avoided crossings are observed because now $(0, 1)_{Sector} > (4, 0)_D$.

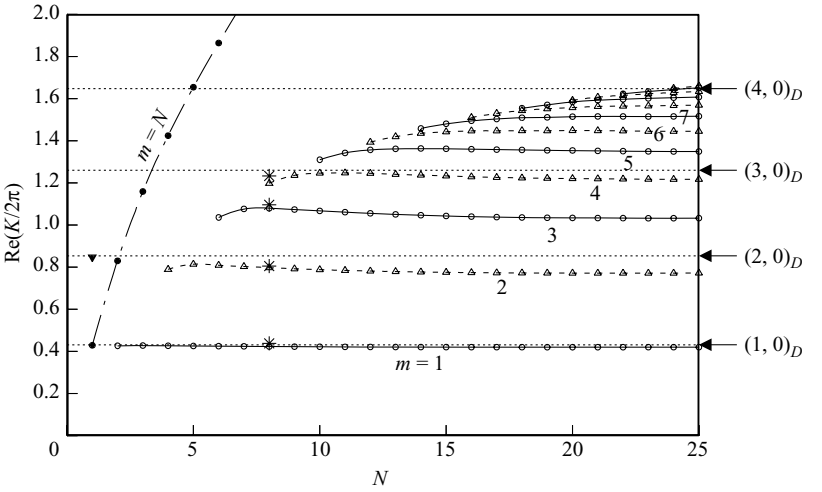

FIGURE 7. Annular cascade with radial plates of length $l/D = 0.25$, thickness $s/D = 0.02$ and hub-to-tip ratio $d/D = 0.5$: variation of $(m, 0, 0)$ trapped mode frequencies $\mathrm{Re}(K/2\pi)$ as function of blade number N. The asterisk symbols depict the experimental results of Parker & Pryce (1974) for $N = 8$. $p = 2$, $d_{PML} = 2$, $\sigma_0 = 2$, $\Delta = 0.05/0.14$.

4.2. *Influence of blade number*

Next we consider the influence of blade number N on the trapped mode frequencies in figure 7. We see that with increasing blade number N more and more trapped modes appear exactly as predicted by Duan & McIver (2004), namely for even number of blades $N/2 + 1$ trapped modes $(m, 0, 0)$ exist whereas for odd number of blades $(N - 1)/2 + 1$ trapped modes $(m, 0, 0)$ are possible. With increasing m the trapped mode frequencies are significantly below the corresponding duct cutoff frequencies $(m, 0)_D$ as can be seen in figure 7. The $m = N$ trapped mode with the highest frequency always has N wavelengths around the circumference and appears to be always a standing wave. All others are spinning modes with the exception of the trapped mode with the second highest frequency which corresponds to the 'one node per blade' mode. Aside from the $m = N$ trapped mode the trapped mode frequencies remain almost constant with increasing blade number N. For the (unrealistic) case of $N = 1$ we computed an additional $m = 2$ mode with very low damping (depicted by the filled upside down triangle in figure 7) which might also be a truly trapped mode because its frequency is slightly below the duct cutoff frequency $(2, 0)_D$ (for the corresponding infinitely thin radial fin case with $d/D = 0$ and $N = 1$ Linton & McIver (1998) mentioned only the $m = 1$ trapped mode).

4.3. *Influence of blade stagger*

Another important cascade parameter is the stagger angle α. In an actual compressor cascade the stagger angle varies with radius. For simplicity, we keep the stagger angle constant over the radius and are merely interested in the trend as α increases. For staggered plates, no symmetry exists and we have to use the full geometry in our computation. Figure 8 shows the dependence of frequency of the first four trapped modes $(m, 0, 0)$, $m = 1, \ldots, 4$ on the stagger angle for $0^\circ \leqslant \alpha \leqslant 80^\circ$. The resonant frequency increases slightly with stagger angle α similar to the results of Koch (1983) for a two-dimensional cascade. As can be expected the trapped mode frequencies approach the corresponding duct cutoff frequencies $(m, 0)_D$ as $\alpha \to 90^\circ$ (because for

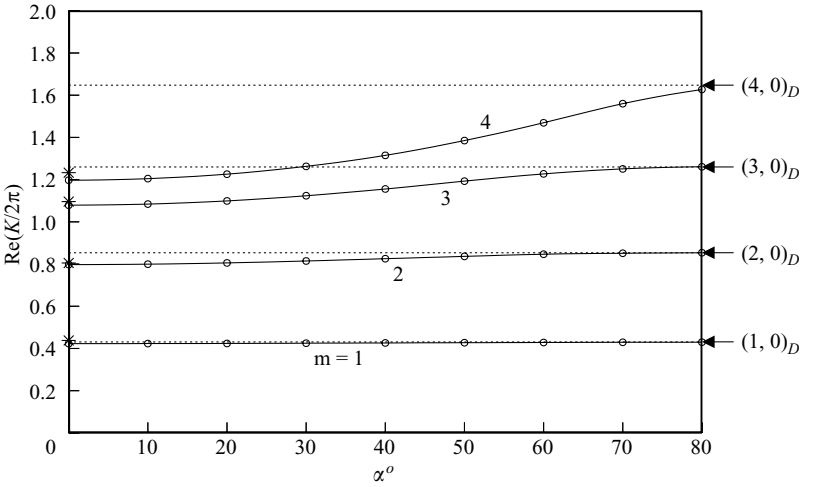

FIGURE 8. Annular cascade with $N = 8$ radial plates of length $l/D = 0.25$, thickness $s/D = 0.02$ and hub-to-tip ratio $d/D = 0.5$: variation of first four trapped mode frequencies $\mathrm{Re}(K/2\pi)$ as function of stagger angle α. The asterisk symbols depict the experimental results of Parker & Pryce (1974) for $\alpha = 0°$. $p = 2$, $d_{PML} = 2$, $\sigma_0 = 2$, $\Delta = 0.06/0.16$.

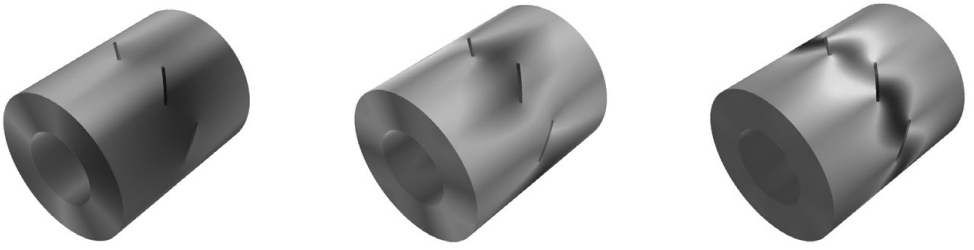

FIGURE 9. First three eigenfunctions of figure 5 but with $\alpha = 50°$ instead of $\alpha = 0°$. The eigenfunctions are depicted between the upstream and downstream PML.

$\alpha = 90°$ and large enough N the blades act like a solid wall resulting in a semi-infinite annulus). Only the higher circumferential modes show noticeable frequency changes with α. Parker (1997) mentioned that for non-zero stagger the agreement between experiments and theoretical predictions is generally not good because in some theories incorrect assumptions are made as regards the configuration of the nodes upstream and downstream of the cascade. Experimentally the nodes are found in planes normal to the cascade. Figure 9 shows the first three eigenfunctions of figure 5 but for a stagger angle $\alpha = 50°$. The (1, 0, 0) mode is still very close to the duct cutoff frequency, but the (4, 0, 0) mode clearly shows a node approximately normal to the plates.

4.4. *Influence of blade sweep and blade taper*

In modern turbofan engines vane sweep is used as a passive means of reducing vortex-stator interaction tone noise, see for example, Schulten (1997), Envia & Nallasamy (1999), Woodward *et al.* (2001), Elhadidi & Atassi (2005) and Cooper & Peake (2006). Furthermore, Fric *et al.* (1998) demonstrated that tapered chord struts effectively reduce the noise in an annular exhaust diffuser of an industrial gas turbine by uncoupling vortex shedding from acoustic resonant response. One has to distinguish

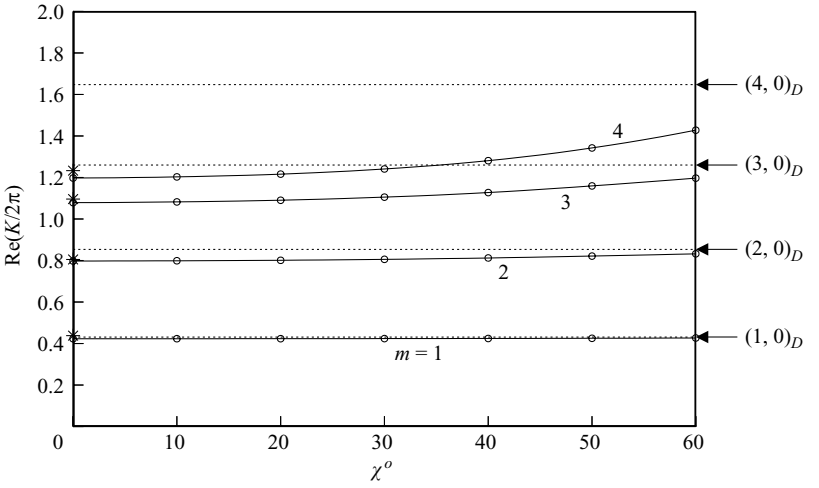

FIGURE 10. Annular cascade with $N = 8$ swept plates of length $l/D = 0.25$, thickness $s/D = 0.02$ and hub-to-tip ratio $d/D = 0.5$: variation of first four trapped mode frequencies $\mathrm{Re}(K/2\pi)$ as function of sweep angle χ. The asterisk symbols depict the experimental results of Parker & Pryce (1974) for $\chi = 0°$. $p = 2$, $d_{PML} = 2$, $\sigma_0 = 2$, $\Delta = 0.06/0.16$.

between reducing the sound source and enhancement of an existing sound source by acoustic resonances. In the present paper we are only concerned about the latter, and therefore investigate the effect of blade sweep and blade taper on the trapped mode frequencies. For simplicity, we consider $N = 8$ swept or tapered plates of finite thickness s/D and chord length l/D at the hub equally distributed around the circumference of an annular duct as sketched in the lower left-hand side of figure 1.

Figure 10 shows the variation of the trapped mode frequencies with increasing sweep angle χ. Again we have a slight increase of frequency towards the duct cutoff frequency $(m, 0)_D$ which is more pronounced for the higher circumferential modes. For the influence of taper we consider again $N = 8$ plates of thickness s/D and chord length l/D at the hub with combined leading and trailing-edge taper of equal taper angle $\gamma = \gamma_l = -\gamma_t$. The results for the first four trapped mode frequencies are shown in figure 11. The trapped mode frequencies increase towards the corresponding duct cutoff frequencies $(m, 0)_D$. In this context it is of interest to note that Fric *et al.* (1998) also observed a shift of peak amplitude frequency to higher frequencies with increasing taper which might indicate that in their experiment the acoustic resonances indeed controlled the vortex shedding.

5. Tandem plate cascades in annular duct

To obtain a better understanding of blade interaction noise in axial flow compressors Parker and his co-workers carried out detailed experiments with fixed tandem plates (Stoneman *et al.* 1988) as well as fixed annular tandem cascades (Legerton *et al.* 1991). Johnson & Loehrke (1984) had studied the sound generation by vortex shedding from tandem plates in an open jet and showed that plate spacing is an important parameter. The results depended on whether the wake was laminar or turbulent. For laminar wakes they observed a typical flow resonant feedback mechanism similar to that described by Rockwell (1983) (compare also Lamoureux & Weaver 1991): for constant flow velocity (i.e. constant Reynolds number) the frequency

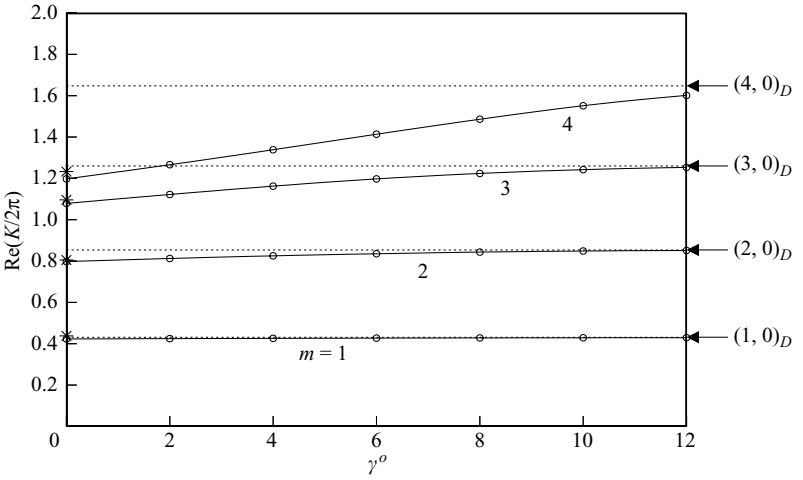

FIGURE 11. Annular cascade with $N=8$ tapered plates of length $l/D=0.25$, thickness $s/D=0.02$ and hub-to-tip ratio $d/D=0.5$: variation of first four trapped mode frequencies $\mathrm{Re}(K/2\pi)$ as function of taper angle γ. The asterisk symbols depict the experimental results of Parker & Pryce (1974) for $\gamma=0^\circ$. $p=2$, $d_{PML}=2$, $\sigma_0=2$, $\Delta=0.06/0.16$.

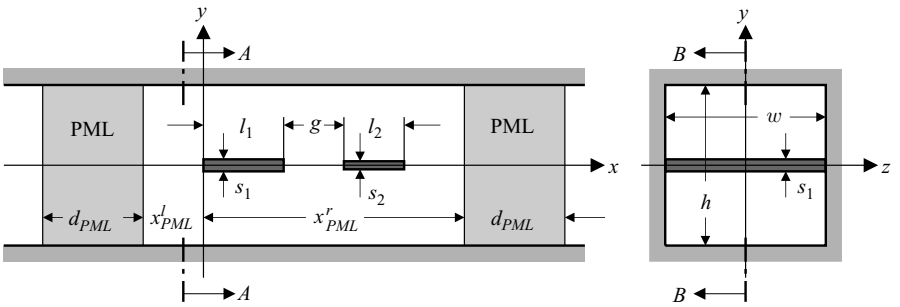

FIGURE 12. Sketch of tandem plates in rectangular duct with PMLs.

showed a saw-tooth-like behaviour with increasing plate separation and the amplitude varied cyclically with plate separation. For constant plate separation a typical frequency staging was observed with increasing flow velocity. For turbulent flow and outside the vortex formation region the frequency was independent of plate separation, and no feedback mechanism was observed although the amplitude of the sound varied periodically with plate spacing. Stoneman *et al.* (1988) introduced an acoustic resonator by enclosing the tandem plates in a hard-walled duct. In this case the resonant frequency dominated the vortex shedding and large-amplitude noise occurred over considerably wider lock-in ranges (compare the similar observations by Mohany & Ziada (2005) for tandem cylinders in a duct). Similar extended lock-in ranges were observed in annular cascades by Legerton *et al.* (1991) and in axial flow compressors by Parker & Stoneman (1987). Therefore it is of importance to predict the resonant frequencies in order to avoid possibly dangerous frequency ranges.

5.1. *Tandem plates in rectangular duct*

Before treating annular tandem cascades we reconsider the model problem of Stoneman *et al.* (1988) namely two plates located in tandem on the centreline of a rigid-walled duct of square cross-section $h^*=w^*=244\,\mathrm{mm}$ as depicted in figure 12.

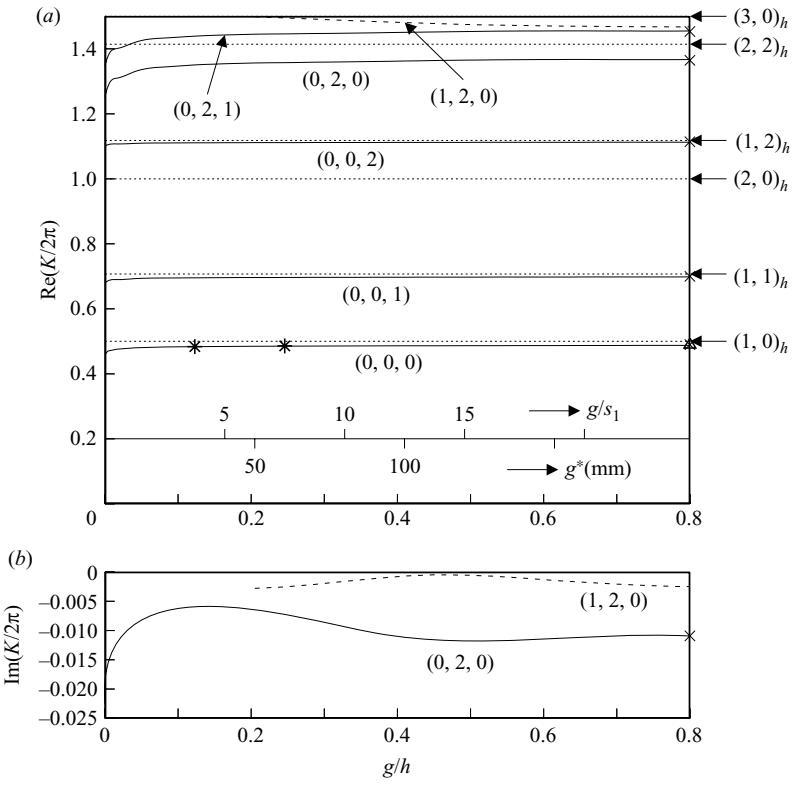

FIGURE 13. Tandem plates of Stoneman *et al.* (1988) in square duct: (*a*) resonant frequencies $\mathrm{Re}(K/2\pi)$ of (n_x, n_y, n_z) modes as function of gap g/h between plates. (*b*) damping $\mathrm{Im}(K/2\pi)$ of (0, 2, 0) and (1, 2, 0) modes as function of gap g/h. The asterisk symbols depict the experimental results of Stoneman *et al.* for Parker's β mode (0, 0, 0) at $g^* = 30$ mm and $g^* = 60$ mm. The triangular symbol at $g/h = 0.8$ shows the experimental result for the upstream plate alone and the cross symbols depict our corresponding computational results. The arrows on the right-hand side of figure 13(*a*) mark the cutoff frequencies of the square duct. $p = 2$, $d_{PML} = 2$, $\sigma_0 = 2$, $\Delta = 0.08/0.16$.

For this problem the reference length l^*_{ref} is appropriately chosen as h^*. The first plate has a chord length of $l^*_1 = 66.7$ mm and a thickness of $s^*_1 = 8$ mm. The downstream plate has a chord length of $l^*_2 = 40$ mm and a thickness of $s^*_2 = 5$ mm. The second plate could be moved in the downstream direction leaving a variable gap g^* between the first and the second plate. Instead of the semicircular leading and trailing edges of the plates used by Stoneman *et al.*, we chose plates of rectangular cross-section because the rounding is of no influence on the resonances (note however that it is important for the source mechanism). Similar to the annular duct treated in the previous section all resonant modes are classified by three numbers (n_x, n_y, n_z) where n_x denotes the number of nodal lines in x direction, n_y the number of nodal lines in y direction at the plate location and n_z the number of nodal lines in z direction. Parker's β mode, which has opposite phase across the plate, is then simply (0, 0, 0). The results of our numerical computation are shown in figure 13.

As noted by Stoneman *et al.* (1988), for zero spacing the resonant frequencies are those for a single plate of the combined chord lengths and therefore lower. For increasing gap between the two plates the resonant frequencies rapidly increase and

asymptote towards the resonant frequencies of the plate with the larger chord, which is the upstream plate (in figure 13 the single-plate results are depicted by cross symbols at $g/h = 0.8$). Nothing has been said about the downstream plate with the shorter chord. However, for large enough spacing the resonant frequencies of both plates should show up asymptotically. This question can be resolved by assuming that both plates have the same chord length and thickness, as discussed in figure 16 of Hein *et al.* (2004) for the two-dimensional case. Then a symmetry about the middle of the gap exists, and besides Parker's x-symmetric β mode also Parker's x-antisymmetric α mode is possible albeit only for larger chord lengths. That is exactly what is happening here: for larger gaps additional modes appear which have a nodal line in x direction and whose frequencies asymptote for large gap towards the resonant frequencies of the downstream plate with the shorter chord. In our case this is the higher order resonant mode (1, 2, 0) in figure 13 which is depicted by a dashed curve. The frequency of mode (1, 2, 0) increases with decreasing gap width and ends at the duct cutoff frequency $(0, 3)_h \equiv (3, 0)_h$ for g/h approaching 0. Besides Parker's two-dimensional trapped β mode (0, 0, 0) also three-dimensional trapped modes $(0, 0, n)$, $n = 1, 2, \ldots$ with n nodal lines in z direction exist. But these are apparently not excited at the flow velocities used in the experiment of Stoneman *et al.* All these trapped mode frequencies are below the relevant cutoff frequencies $(1, n)_h$, $n = 0, 1, 2, \ldots$ of the square duct which are marked by arrows on the right-hand side of figure 13(*a*). Furthermore, higher order two- and three-dimensional resonant modes also exist, such as (0, 2, 0) and (0, 2, 1). However, these are highly damped as can be seen in figure 13(*b*). For better comparison with the results of Stoneman *et al.* we also included scaled abscissae for the gap g^* in millimetre as well as the ratio g/s_1. The experimental results of Stoneman *et al.* for Parker's β mode at $g^* = 30$ mm and $g^* = 60$ mm (their figure 12), computed with $c_0^* = 343$ m s^{-1}, are marked by asterisk symbols in our figure 13(*a*). At $g/h = 0.8$ we plotted the experimental result of Stoneman *et al.* for the upstream plate only (their figure 9) and marked our corresponding computational results by cross symbols. The agreement is quite good despite the zero mean flow assumption in our computation. Furthermore, we see that at $g/h = 0.8$ the tandem plate results are practically identical with the results for the upstream plate only.

Another experiment with tandem plates in a rectangular duct has been described by Legerton (1992) in his voluminous PhD thesis. This thesis is hard to get and after month-long fruitless attempts I obtained a copy only through the helpful intervention of Stewart Stoneman. As Legerton identified three-dimensional trapped β modes, we also compute the resonances for his geometry in the following. His rectangular duct was $h^* = 200$ mm high and $w^* = 100$ mm wide and l_{ref}^* is taken to be h^*. The first plate had a length of $l_1^* = 100$ mm and was $s_1^* = 8$ mm thick. Legerton considered various lengths for the downstream plate, all $s_2^* = 5$ mm thick, but his most extensive tests were with a plate of length $l_2^* = 20$ mm which will be used in our resonance computation. The results for the resonant frequencies are shown in figure 14.

The modes $(0, 0, n_z)$, $n_z = 0, 1, 2, \ldots$, are apparently trapped modes below the corresponding duct cutoff frequencies $(1, n_z)$, $n_z = 1, 2, \ldots$, marked on the right-hand side of figure 14. All other modes are damped. The asterisk symbols show the experimental results of Legerton (1992) for Parker's β mode (0, 0, 0) as well as the three-dimensional Parker mode (0, 0, 1), extracted from Legerton's figure 5.9, for several gaps between the two plates and assuming $c_0^* = 340$ m s^{-1}. The results for the first plate alone, taken from Legerton's figure 5.1, are plotted at $g/h = 0.5$ as triangular symbols and the cross symbols give our corresponding computational results. For the single upstream plate Legerton found an additional mode at 3690 Hz (see his figures

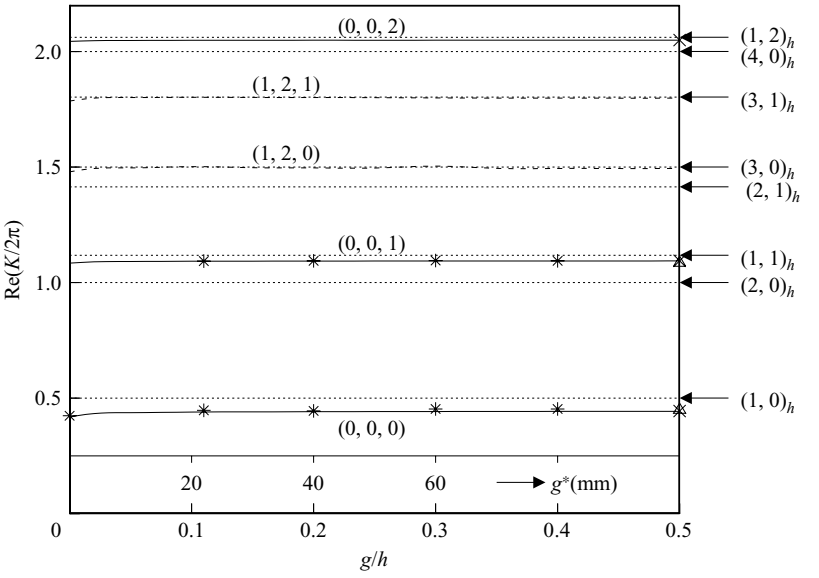

FIGURE 14. Tandem plates of Legerton (1992) in rectangular duct: resonant frequencies $\mathrm{Re}(K/2\pi)$ of (n_x, n_y, n_z) modes as function of gap g/h between plates. The asterisk symbols depict the experimental results of Legerton for Parker's β mode (0, 0, 0) and the three-dimensional Parker mode (0, 0, 1) at $g^* = 22$ mm, 40 mm, 60 mm, 80 mm. At $g^* = 100$ mm the experimental results of Legerton for the upstream plate alone are marked by triangular symbols and our corresponding computational resonances by cross symbols. The arrows on the right-hand side of figure 14 mark the cutoff frequencies of the rectangular duct. $p = 2$, $d_{PML} = 2$, $\sigma_0 = 2$, $\Delta = 0.06/0.16$.

FIGURE 15. First three trapped mode eigenfunctions for the tandem plates in a rectangular duct for the geometry of Legerton (1992) with $g^* = 100$ mm. The eigenfunctions are depicted between the upstream and downstream PML.

5.1 and 5.2) which he identified as antisymmetric about $x = 0$, symmetric about $y = 0$ and with two nodes in z direction. A mode with an antinode in the plane of the plate is unusual and we could not find such a mode with low damping, but the frequency is close to our (0, 0, 2) trapped mode which is antisymmetric about $y = 0$ as all Parker modes. To demonstrate this we depict the computed eigenfunctions for the first three trapped modes at $g^* = 100$ mm in figure 15. The (0, 0, 0) and (0, 0, 1) modes agree very well with our resonance computation. For better comparison with the experiment of Legerton we again included an additional axis in figure 14 giving the gap g^* in mm.

In summary, we can say that the acoustic trapped mode resonances of tandem plates in a rectangular duct control the vortex shedding frequency through lock-on.

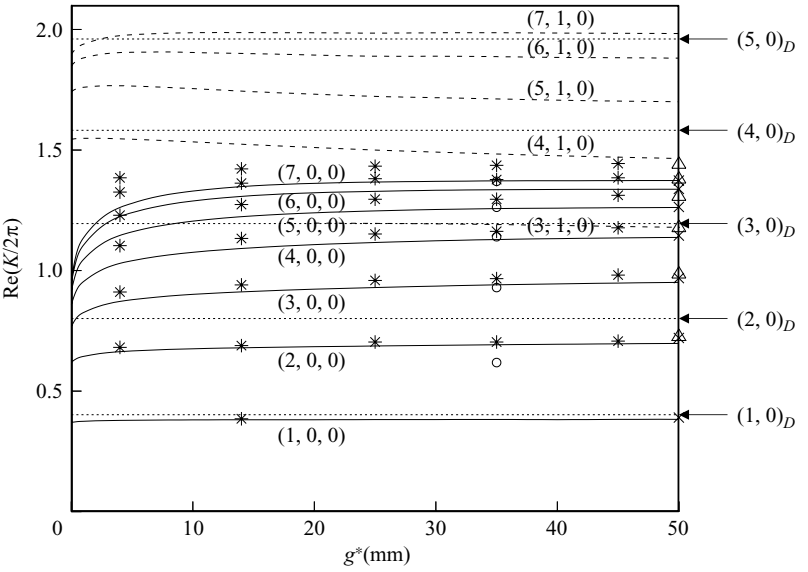

FIGURE 16. Tandem cascades of Legerton (1992) in annular duct: resonant frequencies $\mathrm{Re}(K/2\pi)$ of trapped modes $(m, n, 0)$ as function of gap g^*[mm] between cascades. The asterisk symbols depict some of the experimental results of Legerton. The triangular symbols at $g^* = 50$ mm show the experimental results of Legerton for the single upstream cascade. The circular symbols at $g^* = 35$ mm depict the theoretical results of Woodley & Peake (1999*a*). $p = 2$, $d_{PML} = 2$, $\sigma_0 = 2$, $\Delta = 0.08/0.16$.

The periodic increase and decrease of the modal amplitude with increasing gap width, as observed by Stoneman *et al.* (1988) and Legerton (1992), is due to the feedback mechanism between the vortices shed from the first plate and the vortices impinging on the leading edge of the second plate.

5.2. *Tandem cascades in annular duct*

Legerton (1992), with first results published in Legerton *et al.* (1991), performed experiments also with fixed annular plate cascades in tandem with a variable gap between them, and we shall use his geometry for our numerical computations of the acoustic resonances (compare figure 1 for our notation). Legerton's annular duct with $d/D = 0.6$ had an outer diameter $D^* = 254$ mm(10 in.) and inner diameter $d^* = 152.4$ mm(6 in.). The upstream cascade consisted of $N = 15$ plates of chord length $l_1^* = 69.9$ mm and thickness $s_1^* = 3.8$ mm. The downstream cascade also consisted of $N = 15$ plates which were of chord length $l_2^* = 40$ mm and $s_2^* = 3$ mm thick. Instead of the semicircular edges of the upstream plates and the semicircular leading edge and asymmetrically bevelled trailing edge of the downstream plates used by Legerton, we chose rectangular plates because the edge form is of negligible influence for the resonances. However, we note again that the edge form is of vital influence for the vortex shedding source mechanism. Our computed resonant frequencies for $0\,\mathrm{mm} \leqslant g^* \leqslant 50\,\mathrm{mm}$ are compared with the experimental results of Legerton in figure 16.

Qualitatively, the results are very similar to those for the tandem plates in the previous subsection, only instead of the three-dimensional modes (n_x, n_y, n_z) with the number n_z of nodal points of a mode across the channel we have now our annular modes (m, n, ρ) with the circumferential mode number m. Here n is the axial mode

number and ρ denotes the radial mode number. For zero gap $g^* = 0$ mm the tandem cascade reduces to a single cascade with the combined chord length and eight trapped modes $(m, 0, 0)$, compare figure 7, seven of which are shown in figure 16. For $g^* > 0$ these trapped modes are depicted by solid curves which for $g^* \to \infty$ quickly asymptote towards the trapped modes for the single upstream cascade with the larger chord length $l_1^* = 69.9$ mm , marked by the cross symbols at $g^* = 50$ mm. For $g^* = 0$ also modes $(m, 1, 0)$ exist with one axial node. These are depicted by the dashed curves which for $g^* \to \infty$ asymptote towards the trapped modes of the single downstream cascade with the smaller chord length $l_2^* = 40$ mm. It is also of interest to note that we did not observe any nearly trapped modes which could be attributed to oscillations in the gap between the two cascades. Only the continuous spectra, beginning at the cutoff frequencies $(m, 0)_D$ in the empty annulus, show up in discrete form due to our numerical treatment.

The asterisk symbols in figure 16 depict the experimental results of Legerton (1992) extracted from his figure 5.30 for $g^* = 4$ mm, 14 mm, 25 mm, 35 mm and $g^* = 45$ mm assuming $c_0^* = 343$ m s^{-1}. With increasing frequency Legerton observed 7 circumferential modes with increasing m which are to be compared with our computed solid curves for the $(m, 0, 0)$ modes. However, in his experiment the $m = 1$ mode was excited only for a few gaps such as the one shown at $g^* = 14$ mm. The eighth trapped mode $m = 15$ has a much higher frequency which is outside their measured frequency domain. Legerton observed two $m = 7$ modes, however their exact origin is not clear; in figure 16 we only plotted the first $m = 7$ mode. All experimental resonant frequencies asymptote quickly towards the resonant frequencies of the single upstream cascade depicted by triangular symbols at $g^* = 50$ mm. We observe that the resonant frequencies, in particular those of the higher m modes, are far below the relevant duct cutoff frequencies marked by the arrows on the right-hand side of figure 16. Whereas the lower circumferential modes agree fairly well with our computed resonances, depicted by the solid curves, there is a discrepancy between our numerical and the experimental values which increases with increasing m. The same trend can be observed between the experimental (triangular symbols) and computational (cross symbols) results for the upstream cascade alone plotted at $g^* = 50$ mm (actually it can also be seen in figure 4 for $N = 8$ and $d/D = 0.5$). The reason for this discrepancy is still unclear. From Koch (1983) one would expect even lower resonant frequencies if mean flow were included in our analysis such that neglecting mean flow can be excluded as reason. Another reason could be inadequate grid resolution. We therefore considered half the single upstream plate using symmetry about $x = 0$ and halved the mesh size from $\Delta = 0.08/0.16$ to $\Delta = 0.04/0.16$. The result did not change. Then we doubled the length of the PML to be $d_{PML} = 4$ instead of $d_{PML} = 2$, and again there was no change in the result. We therefore conclude that the above mentioned discrepancy is not due to inadequate accuracy in our computation.

The only available theoretical computation of acoustic resonances is by Woodley & Peake (1999*a*) who compared their results with those of Legerton (1992) for $g^* = 35$ mm in their figure 9. Woodley & Peake used a straight cascade with plates of zero thickness but included mean flow. Their results are depicted in our figure 16 by circular symbols at $g^* = 35$ mm. Woodley & Peake calculated resonant states for the modes $m = 2, \ldots, 6$ by finding the zeros of the truncated infinite-dimensional scattering matrix. However, it might be that their $m = 6$ mode is actually the $m = 7$ mode. Their lowest mode $m = 2$ is apparently affected by their assumption of small annulus curvature but otherwise the results of Woodley & Peake are fairly close to our numerical results.

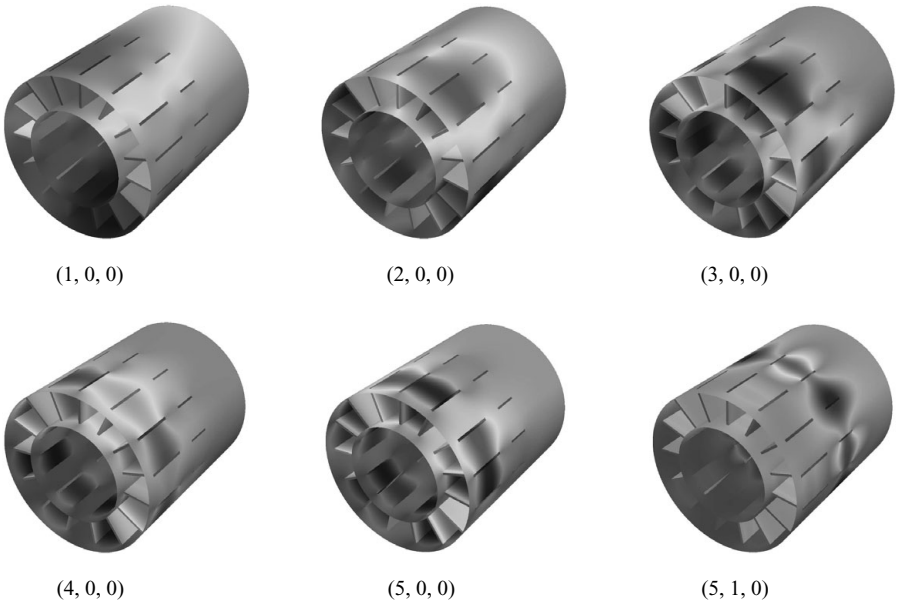

FIGURE 17. First five trapped mode eigenfunctions $(m, 0, 0)$ and the eigenfunction $(5, 1, 0)$ for the annular tandem cascades of Legerton (1992) with $g^* = 35\,\text{mm}$.

We also computed the family of modes with one node in axial direction, i.e. $(m, 1, 0)$ with $m = 1, \ldots, 7$, depicted by the dashed curves in figure 16. Apparently these resonances were not excited in the experiment of Legerton (1992). In figure 17 the eigenfunctions of several trapped modes for $g^* = 35\,\text{mm}$ of figure 16 are depicted. The domain of the shown eigenfunctions is cut in front of the first plate cascade to give a view inside the cascade and ends at the beginning of the downstream PML.

Legerton (1992) also carried out tests with a circumferential offset between the upstream and downstream cascade and found a substantial amplitude reduction or even disappearance of modes when the offset was greater than one upstream plate thickness. Furthermore, he no longer observed the cyclic variation in the amplitude with axial spacing. This can be attributed to a reduction of the exciting source, namely the wake impingement on the leading edge of the downstream cascade, because our resonance computation with a 12° offset between the upstream and downstream cascade, i.e. half a pitch, gave almost identical trapped mode frequencies as for zero offset. This indifference of the trapped mode frequencies to circumferential offset suggests that the resonances might not change significantly even if one of the cascades rotates, i.e. in an actual compressor. However, the source mechanism changes if one of the cascades rotates as demonstrated by Tyler & Sofrin (1962) (see also Woodley & Peake 1999*b*).

Actual compressors have a different number of blades in adjacent cascades (usually the number of stator blades is larger than the number of rotor blades). Therefore, Legerton (1992) suggested that further tests should be performed with a dissimilar number of plates in each row. With our numerical method this can easily be done. First, we keep the number $N_1 = 15$ of the upstream plates with the larger chord length fixed and vary the number N_2 of the downstream plates. The results are shown in figure 18 for $0 \leqslant N_2 \leqslant 20$. Apparently the frequencies of the trapped modes $(m, 0, 0)$, dominated by the upstream cascade with the larger chord, remain

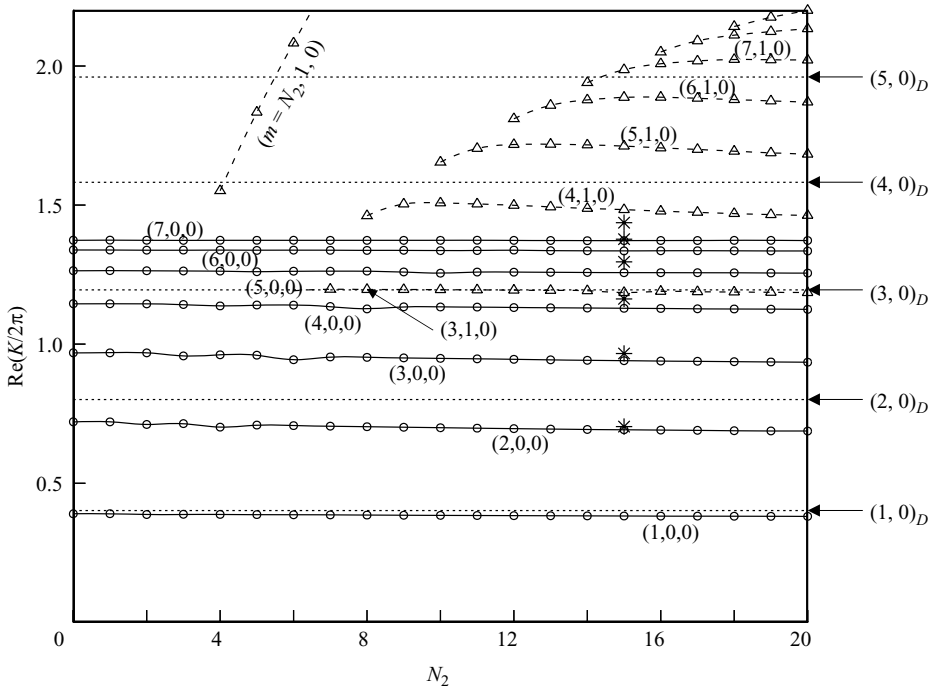

FIGURE 18. Tandem cascades of Legerton (1992) in annular duct with $g^* = 35\,\text{mm}$: resonant frequencies $\text{Re}(K/2\pi)$ of trapped modes with fixed $N_1 = 15$ and variable plate number N_2. The asterisk symbols depict the experimental results of Legerton for $N_2 = 15$. $p = 2$, $d_{PML} = 2$, $\sigma_0 = 2$, $\Delta = 0.08/0.16$.

almost constant whereas the frequencies of the modes $(m, 1, 0)$ follow the trend of figure 7 as $N_2 \to 0$. On the other side, for fixed $N_2 = 15$ and variable N_1 the frequencies of the modes $(m, 0, 0)$ are very similar to those in figure 7 as $N_1 \to 0$. Again, this seems to indicate that the blades with the largest chord length dominate the resonant frequencies in multistage cascades.

6. Conclusion

Vortices or coherent structures shed in the wake of turbomachinery blades may be strongly enhanced or controlled by acoustic resonances resulting in high-amplitude tonal noise or even blade failure. Without resonance the amplitude of shed vortices is limited by nonlinearity. With a resonator the amplitude is limited by the damping of the resonator, i.e. the quality factor Q. Therefore, trapped modes with zero radiation loss ($Q = \infty$), or nearly trapped modes with very low radiation loss, are of particular importance. In the present paper we computed the resonances of single and tandem cascades in circular or annular ducts and observed a finite number of trapped modes. These trapped modes are not only the cause of high-amplitude tonal noise but could possibly be also linked to limiting the stability of a compressor at off-design conditions.

There are two possibilities to avoid such dangerous operating conditions. The first is to eliminate or reduce the exciting source. This is not always possible. Therefore the second method is to detune a dangerous resonance. To do this it is of importance to predict the dangerous frequency domains and know how they can be changed by

the various cascade parameters. In the present paper we investigated stationary single and tandem plate cascade for zero mean flow approximating low-Mach-number flows. The exact blade geometry is of minor importance for the resonances but influences the wake source mechanism decisively. For single cascades the most important cascade parameter turned out to be the chord length l/D. The number of blades N is of importance only in so far as it determines the number of trapped modes. For stationary tandem cascades the cascade with the larger blade chord determines the trapped mode frequencies unless the gap between the two blade rows is very small. This might even be true for multistage compressors but needs to be proved.

Naturally, our zero mean flow assumption as well as considering only stationary tandem cascades are only a first step in an attempt to understand and predict acoustic resonances in actual flow compressors. Whereas variable duct area and finite length hub geometry can easily be included in the present numerical method, the extension to non-zero mean flow with swirl and the interaction of moving rotor and stationary vane cascades are non-trivial and are left for future investigations.

The author is grateful to Stefan Hein for stimulating discussions and various help during this investigation. I am indebted to Bernd Hellmich for providing valuable literature about compressor acoustics. Furthermore, I want to express my sincere thanks to Stewart Stoneman for his help in obtaining a copy of Legerton's PhD thesis.

REFERENCES

Abramowitz, M. & Stegun, I. 1965 *Handbook of Mathematical Functions*. Dover.

Aguilar, J. & Combes, J. 1971 A class of analytic perturbations for one-body Schrödinger Hamiltonians. *Commun. Math. Phys.* **22**, 269–279.

Baslev, E. & Combes, J. 1971 Spectral properties of many body Schrödinger operators with dilation analytic interactions. *Commun. Math. Phys.* **22**, 280–294.

Bérenger, J. 1994 A perfectly matched layer for the absorption of electromagnetic waves. *J. Comput. Phys.* **114**, 185–200.

Berry, M. & Wilkinson, M. 1984 Diabolical points in the spectra of triangles. *Proc. R. Soc. Lond.* A **392** (1802), 15–43.

Callan, M., Linton, C. & Evans, D. 1991 Trapped modes in two-dimensional waveguides. *J. Fluid Mech.* **229**, 51–64.

Camp, T. 1999 A study of acoustic resonance in a low-speed multistage compressor. *ASME J. Turbomach.* **121**, 36–43.

Chew, W. & Weedon, W. 1994 A 3-D perfectly matched medium from modified Maxwell's equation with stretched coordinates. *Microw. Opt. Technol. Lett.* **7** (13), 599–604.

Collino, F. & Monk, P. 1998 The perfectly matched layer in curvilinear coordinates. *SIAM J. Sci. Comput.* **19** (6), 2061–2090.

Cooper, A. & Peake, N. 2006 Rotor-stator interaction noise in swirling flow: stator sweep and lean effects. *AIAA J.* **44** (5), 981–991.

Cumpsty, N. & Whitehead, D. 1971 The excitation of acoustic resonances by vortex shedding. *J. Sound Vib.* **18**, 353–369.

Duan, Y. 2004 Trapped modes and acoustic resonances. PhD thesis, Loughborough University, Loughborough.

Duan, Y., Koch, W., Linton, C. & McIver, M. 2007 Complex resonances and trapped modes in ducted domains. *J. Fluid Mech.* **571**, 119–147.

Duan, Y. & McIver, M. 2004 Rotational acoustic resonances in cylindrical waveguides. *Wave Motion* **39**, 261–274.

Duclos, P. & Exner, P. 1995 Curvature-induced bound states in quantum waveguides in two and three dimensions. *Rev. Math. Phys.* **7** (1), 73–102.

Elhadidi, B. & Atassi, H. 2005 Passive control for turbofan tonal noise. *AIAA J.* **43** (11), 2279–2292.

Envia, E. & Nallasamy, M. 1999 Design selection and analysis of a swept and leaned stator concept. *J. Sound Vib.* **228** (4), 793–836.

Evans, D. 1992 Trapped acoustic modes. *IMA J. Appl. Math.* **49** (1), 45–60.

Evans, D., Levitin, M. & Vassiliev, D. 1994 Existence theorems for trapped modes. *J. Fluid Mech.* **261**, 21–31.

Evans, D. & Linton, C. 1991 Trapped modes in open channels. *J. Fluid Mech.* **225**, 153–175.

Evans, D. & Linton, C. 1994 Acoustic resonance in ducts. *J. Sound Vib.* **173**, 85–94.

Fric, T., Villarreal, R., Auer, R., James, M., Ozgur, D. & Staley, T. 1998 Vortex shedding from struts in annular exhaust diffuser. *ASME J. Turbomach.* **120**, 186–192.

Harari, I., Patlashenko, I. & Givoli, D. 1998 Dirichlet-to-Neumann maps for unbounded wave guides. *J. Comput. Phys.* **143**, 200–223.

Hein, S., Hohage, T. & Koch, W. 2004 On resonances in open systems. *J. Fluid Mech.* **506**, 255–284.

Hein, S., Hohage, T., Koch, W. & Schöberl, J. 2007 Acoustic resonances in a high lift configuration. *J. Fluid Mech.* **582**, 179–202.

Hein, S. & Koch, W. 2008 Acoustic resonances and trapped modes in pipes and tunnels. *J. Fluid Mech.* **605**, 401–428.

Hellmich, B. 2008 Acoustic resonance in a high-speed axial compressor. PhD thesis, Universität Hannover, Hannover.

Hellmich, B. & Seume, J. 2008 Causes of acoustic resonances in a high-speed axial compressor. *ASME J. Turbomach.* **130**, 031003–1–031003–9.

Hislop, P. & Sigal, I. 1996 *Introduction to Spectral Theory*. Springer.

Hu, F. 2004 Absorbing boundary conditions. *Intl J. Comput. Fluid Dyn.* **18** (6), 513–522.

Johnson, C. & Loehrke, R. 1984 An experimental investigation of wake edge tones. *AIAA J.* **22**, 1249–1253.

Kim, S. & Pasciak, J. 2009 The computation of resonances in open systems using a perfectly matched layer. *Math. Comp.* S0025–5718(09)02227-3.

Koch, W. 1983 Resonant acoustic frequencies of flat plate cascades. *J. Sound Vib.* **88**, 233–242.

Koch, W. 2005 Acoustic resonances in rectangular open cavities. *AIAA J.* **43** (11), 2342–2349.

Lamoureux, P. & Weaver, D. 1991 The effects of turbulence and damping on pipeline acoustic resonance. *Proc. Inst. Mech. Engrs., Part C* **205**, 303–312.

Legerton, M. 1992 Flow induced acoustic resonances. PhD thesis, University of Wales, Swansea.

Legerton, M., Stoneman, S. & Parker, R. 1991 An experimental investigation into flow induced acoustic resonances in an annular cascade. *Proc. Inst. Mech. Engrs., Part C* **205**, 445–452.

Li, Y. & Mei, C. 2006 Subharmonic resonance of a trapped wave near a vertical cylinder in a channel. *J. Fluid Mech.* **561**, 391–416.

Linton, C. & McIver, P. 1998 Acoustic resonances in the presence of radial fins in circular cylindrical waveguides. *Wave Motion* **28**, 99–117.

Linton, C. & McIver, M. 2002 Periodic structures in waveguides. *Proc. R. Soc. Lond.* A **458**, 3003–3021.

Linton, C. & Ratcliffe, K. 2004 Bound states in coupled guides. I. Two dimensions. *J. Math. Phys.* **45** (4), 1359–1379.

Maniar, H. & Newman, J. 1997 Wave diffraction by a long array of cylinders. *J. Fluid Mech.* **339**, 309–330.

Mohany, A. & Ziada, S. 2005 Flow-excited acoustic resonance of two tandem cylinders in cross-flow. *J. Fluids Struct.* **21** (1), 103–119.

Moiseyev, N. 1998 Quantum theory of resonances: calculating energies, widths and cross-sections by complex scaling. *Phys. Rep.* **302**, 211–293.

Nayfeh, A. & Huddleston, D. 1979 Resonant acoustic frequencies of parallel plates (AIAA–Paper 79–1522). In *Twelfth AIAA Fluid and Plasma Dynamics Conference*, Williamsburg, VA.

Parker, R. 1966 Resonance effects in wake shedding from parallel plates: some experimental observations. *J. Sound Vib.* **4** (1), 62–72.

Parker, R. 1967*a* Resonance effects in wake shedding from compressor blading. *J. Sound Vib.* **6**, 302–309.

Parker, R. 1967*b* Resonance effects in wake shedding from parallel plates: calculation of resonant frequencies. *J. Sound Vib.* **5**, 330–343.

Parker, R. 1968 An investigation of acoustic resonance effects in an axial flow compressor stage. *J. Sound Vib.* **8**, 281–297.

Parker, R. 1984 Acoustic resonances and blade vibration in axial flow compressors. *J. Sound Vib.* **92**, 529–539.

Parker, R. 1997 Aeroacoustics. *Intl J. Fluid Dyn.* **1**, (http://elecpress.monash.edu.au/IJFD), Article 1.

Parker, R. & Griffiths, W. 1968 Low frequency resonance effects in wake shedding from parallel plates. *J. Sound Vib.* **7**, 371–379.

Parker, R. & Pryce, D. 1974 Wake excited resonances in an annular cascade: an experimental investigation. *J. Sound Vib.* **37**, 247–261.

Parker, R. & Stoneman, S. 1985 An experimental investigation of the generation and consequences of acoustic waves in an axial-flow compressor: large axial spacing between blade rows. *J. Sound Vib.* **99** (2), 169–182.

Parker, R. & Stoneman, S. 1987 An experimental investigation of the generation and consequences of acoustic waves in an axial-flow compressor: the effect of variations in the axial spacing between blade rows. *J. Sound Vib.* **116** (3), 509–525.

Parker, R. & Stoneman, S. 1989 The excitation and consequences of acoustic resonances in enclosed fluid flow around solid bodies. *Proc. Inst. Mech. Engrs* **203**, 9–19.

Porter, R. 2007 Trapped modes in thin elastic plates. *Wave Motion* **45**, 3–15.

Porter, R. & Evans, D. 1999 Rayleigh–Bloch surface waves along periodic gratings and their connection with trapped modes in waveguides. *J. Fluid Mech.* **386**, 233–258.

Ragab, S. & Salem-Said, A.-H. 2007 Response of a flat-plate cascade to incident vortical waves. *AIAA J.* **45** (9), 2140–2148.

Rockwell, D. 1983 Oscillations of impinging shear layers. *AIAA J.* **21** (5), 645–664.

Schöberl, J. 1997 NETGEN: an advancing front 2D/3D-mesh generator based on abstract rules. *Comput. Vis. Sci.* **1**, 41–52.

Schulten, J. 1997 Vane sweep effects on rotor/stator interaction noise. *AIAA J.* **35** (6), 945–951.

Simon, B. 1973 The theory of resonances for dilation analytic potentials and the foundations of time dependent perturbation theory. *Ann. Math.* **97**, 247–274.

Stoneman, S., Hourigan, K., Stokes, A. & Welsh, M. 1988 Resonant sound caused by flow past two plates in tandem in a duct. *J. Fluid Mech.* **192**, 455–484.

Tyler, J. & Sofrin, T. 1962 Axial compressor noise studies. *Soc. Automot. Engrs Trans.* **70**, 309–332.

Ulbricht, I. 2002 Stabilität des stehenden Ringgitters. PhD thesis, Technische Universität Berlin, Berlin.

Ursell, F. 1951 Trapping modes in the theory of surface waves. *Proc. Camb. Phil. Soc.* **47**, 347–358.

Utsunomiya, T. & Eatock Taylor, R. 1999 Trapped modes around a row of circular cylinders in a channel. *J. Fluid Mech.* **386**, 259–279.

Woodley, B. & Peake, N. 1999*a* Resonant acoustic frequencies of a tandem cascade. Part 1: zero relative motion. *J. Fluid Mech.* **393**, 215–240.

Woodley, B. & Peake, N. 1999*b* Resonant acoustic frequencies of a tandem cascade. Part 2: rotating blade rows. *J. Fluid Mech.* **393**, 241–256.

Woodward, R., Elliott, D., Hughes, C. & Berton, J. 2001 Benefits of swept-and-leaned stators for fan noise reduction. *J. Aircr.* **38** (6), 1130–1138.

Ziada, S., Oengören, A. & Vogel, A. 2002 Acoustic resonance in the inlet scroll of a turbo-compressor. *J. Fluids Struct.* **16** (3), 361–373.